FERMILAB-PUB-08-452-E

Performance of Silicon Photomultiplers with the CMS HCAL Front-End Electronics

A. Heering and J. Rohlf

Department of Physics, Boston University, Boston, MA 02212, USA

J. Freeman and S. Los

Fermi National Accelerator Laboratory, Batavia, IL 60510, USA

S. Kuleshov

Institute for Theoretical and Experimental Physics, Moscow, Russia

Y. Musienko

Department of Physics, Northeastern University, Boston, MA 02115, USA

Preprint submitted to Elsevier Science *29 June 2006*

Abstract

We have measured the performance of silicon photomultipliers (SiPMs) together with the front-end electronics developed for the Compact Muon Solenoid hadron calorimeter. We find a clean separation of the single PE peak above pedestal noise fluctuations, providing a signal to noise of about 8. The SIPMs may be useful in the near term for readout of the outer (HO) scintillators to significantly enhance the sensitivity to minimum ionizing particles for use in the muon trigger. In the longer term, the SiPMs may be useful for upgrading the detector to accommodate a luminosity upgrade.

Keywords: Silicon PM, SiPM, MRS, APD, HPD, Photodetector

PACS Numbers: 29.40.Mc, 29.40.Vj, 29.90.+r

Please send proofs to:
Adriaan Heering
CERN
CH-1211 Geneve 23
Switzerland
tel.: 41-76-487-4359, fax: 41-22-767-8940, email: Adriaan.Heering@cern.ch

1 Introduction

The avalanche photodiode (APD) and hybrid photodiode (HPD) have long since joined the traditional photomultiplier (PMT) as photodetectors for use in modern high-energy physics experiments[1]. In the past few years, the silicon photomultiplier (SiPM), which is also known as a metal-resister-semiconductor (MRS) structured APD, has emerged as a new candidate with many promising applications[2]-[8]. The general characteristics of the SiPM are high gain ($M = 10^6$), low bias voltage ($V_\mathrm{b} = 40$ V), good photon detection efficiency (30%), single photoelectron (PE) threshold sensitivity, and fast timing (30 ps) in a relatively simple device which works well in a magnetic field. The fundamental characteristics of the various photodetectors are summarized in Table 1. The SiPM is unique amongst the solid-state devices because of its PMT-like gain allowing single photon detection, which is achieved by operation above the breakdown voltage (limited Geiger mode). The size of the sensitive area and low dynamic range of the SiPM, however, may restrict its use in certain applications. The stability of the gain ($\delta M/M$) with a fractional change in bias voltage ($\delta V_\mathrm{b}/V_\mathrm{b}$) is similar for the all the photodetectors, although a greater absolute control of V_b is necessary for the SiPM due to its low operating voltage.

Table 1
Comparison of the APD, HPD, PMT, and SiPM photodetectors. The values for the APD and HPD correspond to devices [1] in use in the calorimeters of the Compact Muon Solenoid, the values for the PMT are typical of many commercially available devices, and the values for the SiPM correspond to the 1-mm^2 devices tested.

	APD	HPD	PMT	SiPM
bias voltage (V_b)	400 V	10 kV	2 kV	40 V
timing (10 PE)	3 ns	100 ps	100 ps	30 ps
sensitivity	10 PE	1 PE	1 PE	1 PE
quantum efficiency	80%	20%	20%	30%
excess noise factor	2.5	1.05	1.1	1.2
dynamic range	10^7	10^7	10^6	10^3
gain (M)	100	2×10^3	10^6	8×10^5
$\delta V_\mathrm{b}/V_\mathrm{b}$ for $\delta M/M$=1%	5×10^{-4}	5×10^{-3}	5×10^{-4}	10^{-3}
δT for $\delta M/M$=1%	0.3°	3.5°	3°	1°

The purpose of the measurements described here was to evaluate the signal-to-noise performance of state-of-the-art SiPMs with existing front end electronics developed for the hadron calorimeter (HCAL)[9] of the Compact Muon Solenoid (CMS)[10] experiment for the CERN Large Hadron Collider (LHC)[11]. One immediate potential application for the SIPM in CMS is to provide larger signal-to-noise for minimum-ionizing particles traversing the HCAL outer scintillators for use in the muon resistive plate chamber (RPC) trigger [12]. A second, longer-range use of the SiPM in CMS could be for the calorimetry readout upgrades that would be necessary for operation of the LHC at an increased luminosity of 10^{35} cm^{-1}s^{-1} [13]-[14].

Two types of SiPMs were tested having different geometries and active areas: 1) 1.1 mm $\times$ 1.1 mm (referred to as 1-mm^2 SiPM), and 2) 2×2 array of 1.1 mm $\times$ 1.1 mm active areas on a single silicon substrate (referred to as 4$\times$ 1-mm^2 SiPM). The SiPMs were manufactured at the Center of Perspective Technology and Apparatus (CPTA) in Moscow, Russia [15].

2 Electronics

The front-end electronics used for these measurements is based on the application specific integrated circuit (ASIC) developed for the Fermilab KTeV experiment[16], modified for analog processing of signals from CMS HCAL at the LHC collision frequency of 40.079 MHz. The ASIC is referred to by its functions of charge integration and encode (QIE)[17]. The CMS version (QIE8) is designed to operate over a wide dynamic range (10^4) with approximately constant precision. The QIE speed is achieved by using 4 identical sets of capacitors so that one bank of capacitors can be integrating, a second settling, a third being digitized and a fourth being read out, resulting in a continuous digital output every 25 ns. The range is achieved by charge integration simultaneously on 4 scales having relative sensitivities of 1, 5, 25, and 125 fC per least count (LC) with output corresponding to the lowest range that is not full scale. A 7-bit grey code format is used, with 5 bits for the mantissa and 2 bits to set the range. The 5-bit mantissa has $15\times1+7\times2+4\times3+3\times4+3\times5$ bins, resulting in a non-linear scale that is summarized in Fig. 1 and Table 2 [18]. The upper curve in Fig. 1 represents the resolution of a CMS-like hadron calorimeter and the contribution of the QIE quantization error can be seen to be negligible.

The QIE8 accommodates positive or negative input polarities so that it can accept signals from HPDs or PMTs as required for the readout of different CMS HCAL sub detectors. For these measurements, we used the negative (PMT) input polarity which has a scale of 2.6 fC per LC.

The QIE has a differential input so that the incoming current pulse is compared a reference input that does not collect signal charge but is sensitve to noise and possible unintended electromagnetic couplings. The signal and reference inputs are processed by identical charge integration circuitry and the flash ADC digitizes the difference between signal and reference providing stability against shifts caused by potential temperature, voltage, and clock frequency variations.

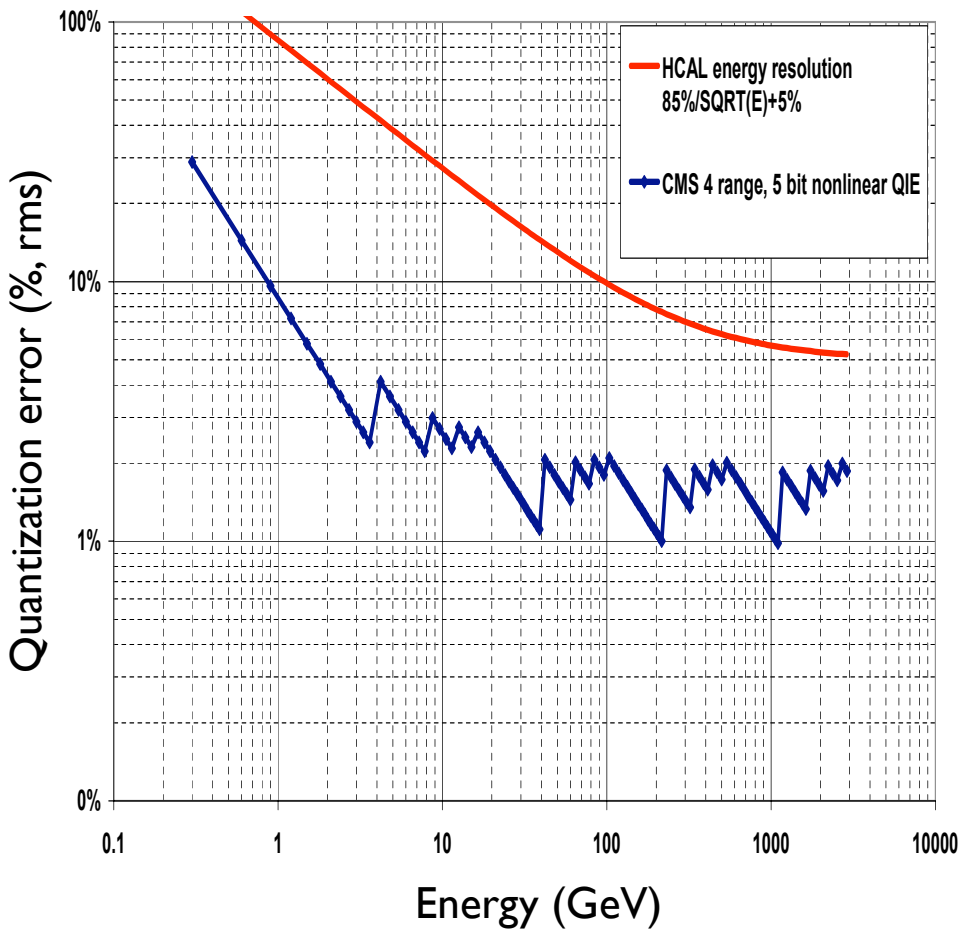

Fig. 1. Quantization error of the QIE8. The binning for each 5-bit mantissa is $15\times1 + 7\times2 + 4\times3 + 3\times4 + 3\times5$. The four ranges are $\times1$, $\times5$, $\times25$, and $\times125$. The contribution of the QIE8 quantization error to the energy resolution of the CMS hadron calorimeter (upper curve) can be seen to be negligible.

Table 2
The QIE8 quantization is done on a nonlinear scale over 128 bins. The least count corresponds to 2.6 fC.

Channel	Bin Size (LC)	gain (fC/LC)	Range (fC)
0-14	1	2.6	0-36
15-21	2	5.2	36-73
22-25	3	7.8	73-104
26-28	4	10.4	104-135
29-46	5	13	135-343
47-53	10	26	343-525
54-57	15	39	525-681
58-60	20	52	681-837
61-78	25	65	837-1877
79-85	50	130	1877-2787
86-89	75	195	2787-3567
90-92	100	260	3567-4347
93-110	125	325	4347-9547
111-117	250	650	9547-14097
118-121	375	975	14097-17997
122-124	500	1300	17997-21897
125-127	625	1625	21897-26772

3 1-mm^2 SiPM Measurements

3.1 SiPM Description

The 1-mm^2 SiPMs (Fig. 2) have an n$^+$-p-p$^+$ stucture optimized for green-red light detection. The SiPM consists of an array of 556 APD pixels of size 45μm $\times$ 45μm providing an active area of 1 mm^2. The pixels are separated by a grid of opaque material, with the fraction of light sensitive area estimated to be about 70%. Figure 3 shows a micrograph of the pixel structure. The device operates with a gain of about 10^6 at approximately 40 V in limited Geiger mode, such that the signal from an individual pixel does not depend on the initial inonization. Since each avalanche is confined to a single pixel, the output signal is proportional to the number of hit pixels and the dynamic range is limited by the total number of pixels. The spectral response is 400-800 nm with peak sensitivity near 600 nm. The signal rise time is about 1 ns with a time jitter of 50 ps. The device is rated for operation in the temperature range $-40°$ to $40°$ C.

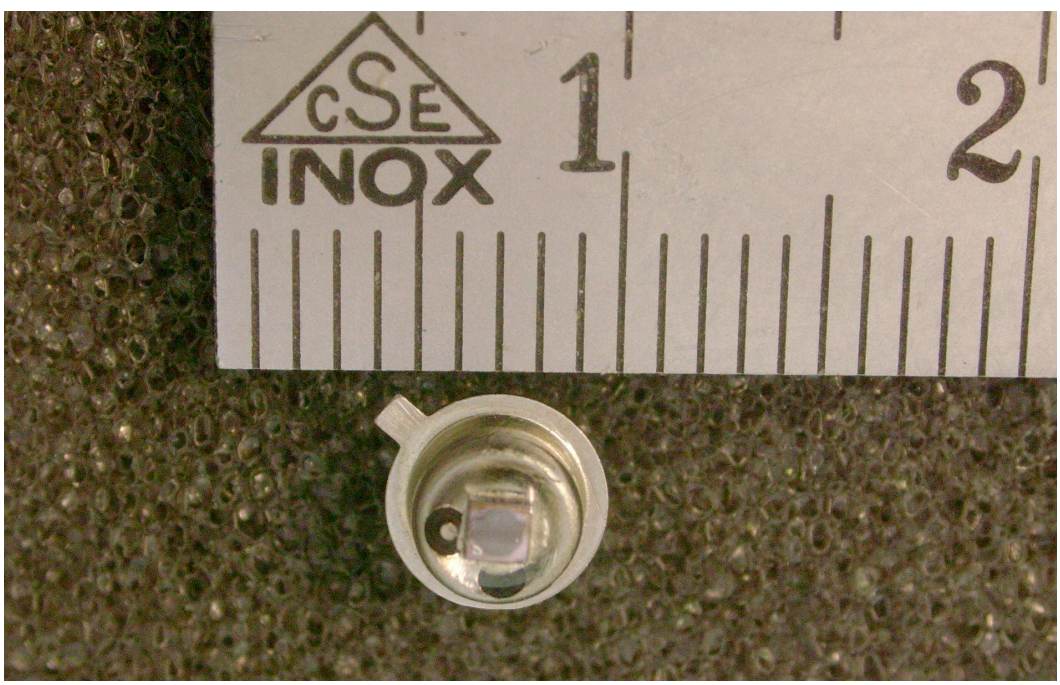

Fig. 2. The 1-mm^2 SiPM.

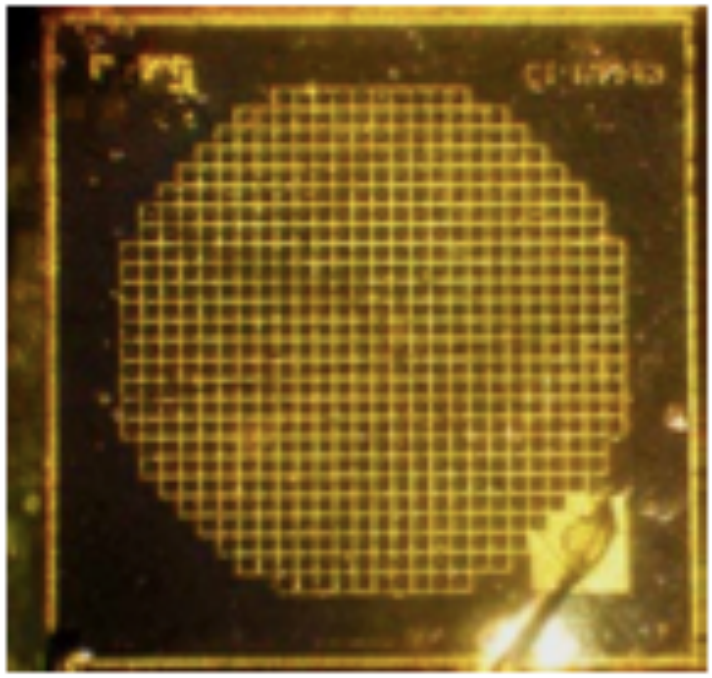

Fig. 3. Micrograph of the 1 mm SiPM. The pixel size is 45μm × 45μm.

3.2 Keithley Power Supply Results

A block diagram of the electronics used to read the SiPM is shown in Fig. 4. The SiPM is connected via a 2-m cable to either the QIE or directly to a scope. The first measurements we describe were made using a Keithley 6487 voltage source rated for 150 μV ripple. The connection to the QIE was made via the 10 pF blocking capacitors as shown in Fig. 4, providing a factor of 5 attenuation.

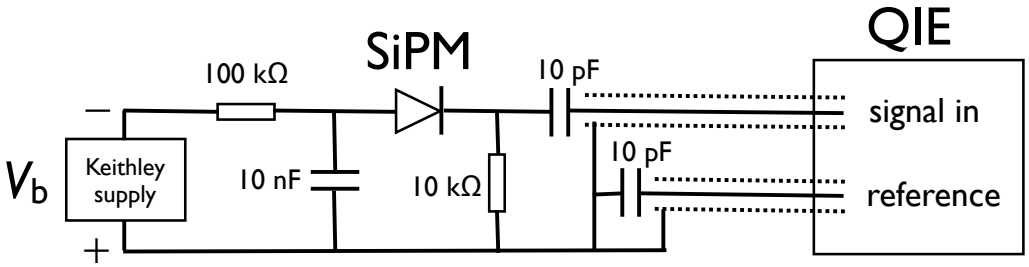

Fig. 4. Block diagram of the electronics for reading the SiPM with the Keithley voltage source. The 10 pF blocking capacitors provide an attenuation of a factor of 5.

Figure 5 shows a scope trace of the signal voltage *vs.* time at 2 mv and 5

ns per division with a 2.5 GHz sampling rate a) without the 10 pF blocking capacitors (no attenuation) and b)with the 10 pF blocking capacitors and the resulting attenuation.

Figure 6 shows the SiPM noise (pedestal) distribution, summed over two consecutive 25-ns time samples, read through the QIE electronics (Fig. 4). The SiPM bias voltage was $V_{\rm b} = 41.8$ V and the current was $I_{\rm b} = 2.2$ μA. The main peak may be fit to a Gaussian giving a mean of 16.3 fC and a root-mean-square (rms) width of 3.6 ± 0.05 fC. The dark current noise is evident as secondary and tertiary peaks approximately 27 and 54 counts above the main (zero-PE) peak corresponding to about 1 MHz of dark counts.

A light emitting diode (LED) was used to deliver an arbitrary but fixed amount light to the SiPM. Figure 7a) shows the average charge digitized by the QIE in 25-ns bins. Twenty time samples are recorded. The average signal of about 70 fC appears in time samples 4 and 5. The relative amount of charge collected in time samples 4 and 5 depends on location of the leading edge of the pulse relative to the 25-ns QIE time sample boundaries. This phase was not adjusted for these measurements. Figure 7b) shows the charge distribution collected in time samples 4 plus 5. Clear peaks are observed for 0, 1, 2, 3, 4, 5, and 6 photoelectrons. The single PE peak, which has an rms width of 3.8 ± 0.08 fC, is observed at 29.9 fC above the zero-PE pedestal peak. Since the pedestal rms width is 3.6 fC, this single PE peak is separated from the noise by about 8σ. The regular separation of the multiple PE peaks indicates a uniformity of the gain consistent with the expectation that the number of hit pixels ($n_{\rm hit}$) is given by

$$n_{\rm hit} = n_{\rm tot}(1 - e^{-f_{\rm n} n_{\rm PE}/n_{\rm tot}}) \approx f_{\rm n} n_{\rm PE} \ ,$$

where $n_{\rm PE}$ is the observed number of PE, $n_{\rm tot}$ is the total number of pixels (556), and $f_{\rm n}$ is the excess noise factor. This corresponds to gain uniformity of order 1% for $n_{\rm PE} < 6$.

3.3 Quantum Efficiency

The quantum efficiency depends not only on production of the first photoelectron in the SiPM active region, but also on the probability of a Geiger discharge which is affected by the bias voltage. Trapping and recombination play a role in making the photon detection efficiency (PDE) both wavelength and bias-voltage dependent. The PDE is further effected by the geometrical factor ($\varepsilon_{\rm g} = 0.7$) due to the opague material separating the SiPM pixels. The spectral dependence of the 1-mm SiPM photon detection efficiency was previously measured [19] at two temperatures, 22° C with $V_{\rm b} = 40.6$ V and and -28°C with $V_{\rm b} = 43$ V. At room temperature, the photon detection efficiency

a)

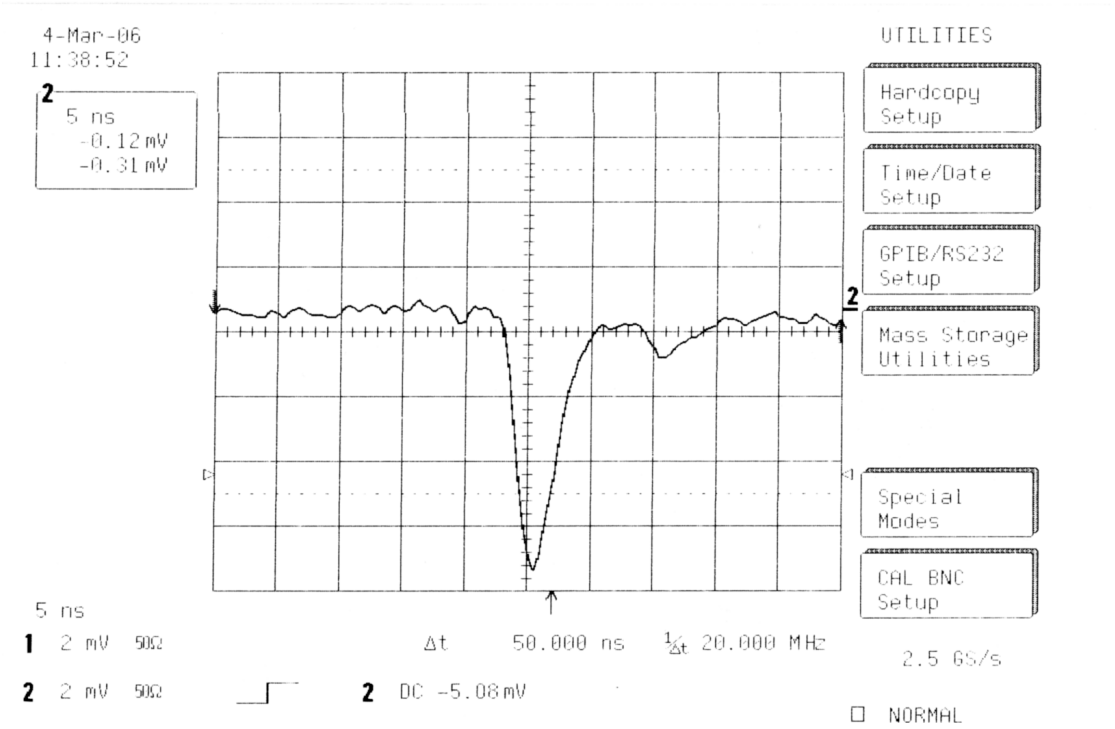

b)

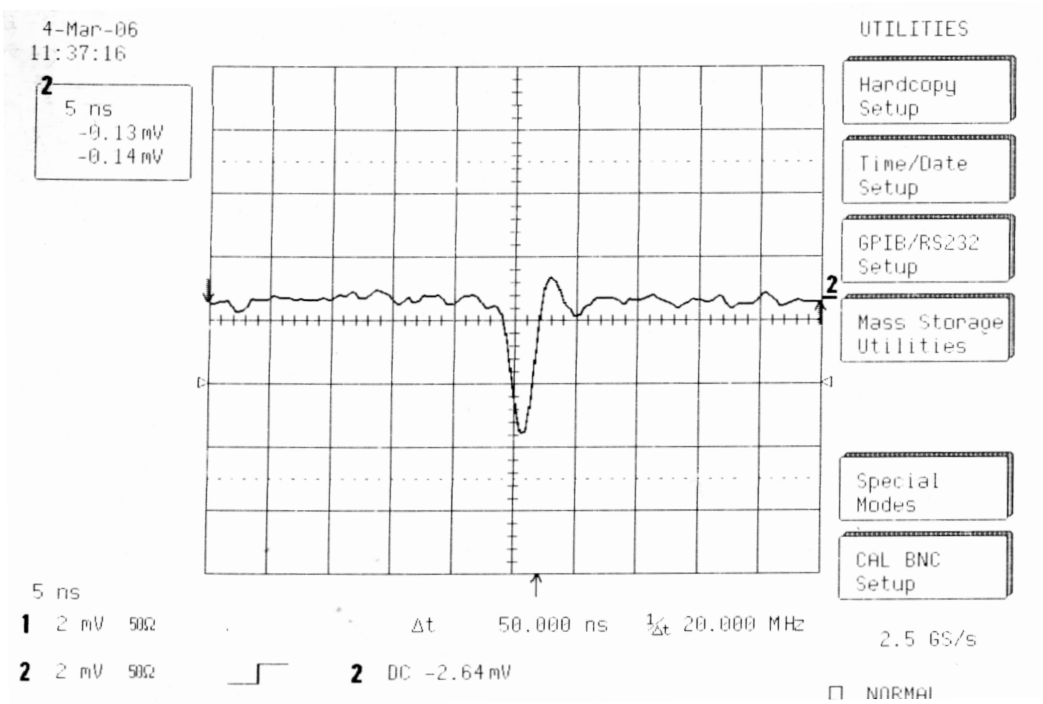

Fig. 5. Signal voltage *vs.* time from the 1-mm^2 SiPM observed with a Lecroy 9361 digital oscilloscope, at 2 mv and 5 ns per division with a 2.5 GHz sampling rate a) without the 10 pF blocking capacitors (no attenuation) and b) with the 10 pF blocking capacitors included (see Fig. 4).

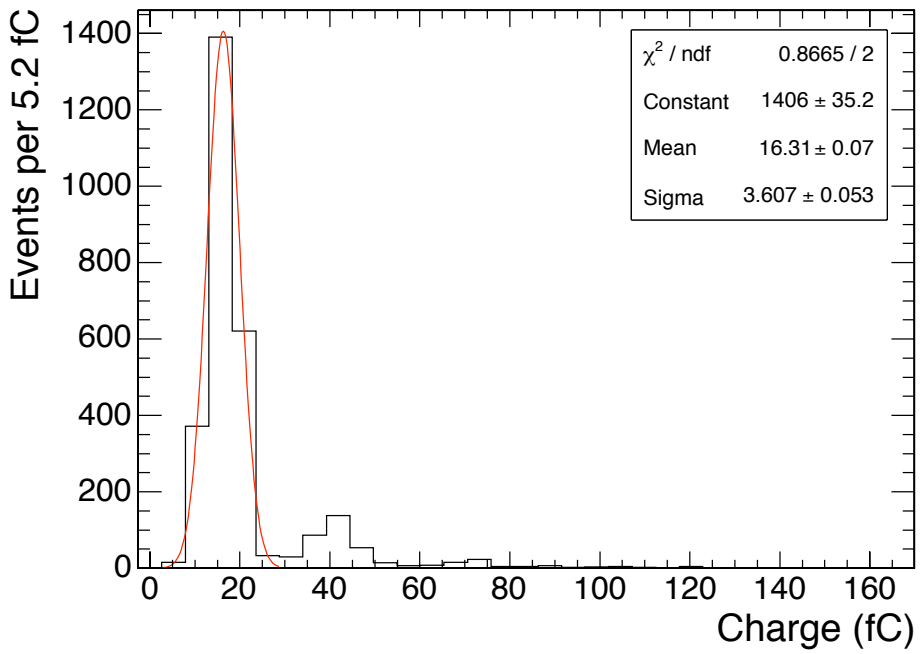

Fig. 6. Pedestal distribution observed with the 1-mm^2 SiPM read through the QIE electronics using the 10 pF blocking capacitors.. The SiPM bias voltage from the Keithley power supply was $V_\mathrm{b} = 41.8$ V and the current was $I_\mathrm{b} = 2.2$ μA. The zero-PE peak is fit to a Gaussian (curve) giving a mean of 16.3 fC and a root-mean-square (rms) width of 3.6 ± 0.05 fC.

is seen to reach 30% at a wavelength of 600 nm (Fig. 8).

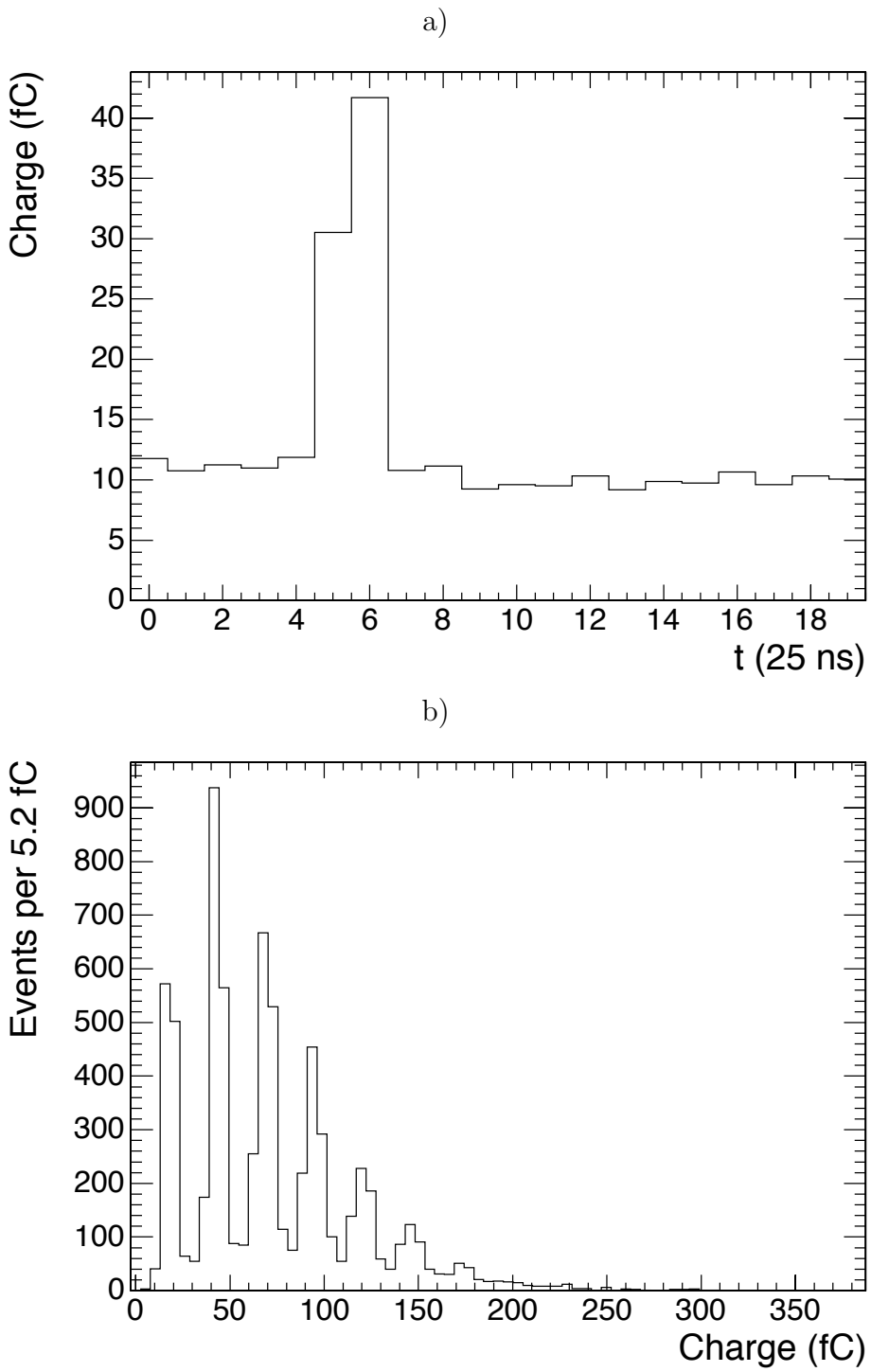

Fig. 7. Pulses from an LED observed with the 1-mm^2 SiPM read through the QIE electronics using the 10 pF blocking capacitors. The SiPM bias voltage from the Keithley power supply was $V_\mathrm{b} = 41.8$ V and the current was $I_\mathrm{b} = 2.2$ μA. a) Charge (Q) *vs.* time (t) collected in 20 25-ns time samples. b) Charge distribution collected in time samples 5 and 6, showing clear peaks for 0, 1, 2, 3, 4, 5, and 6 photoelectrons.

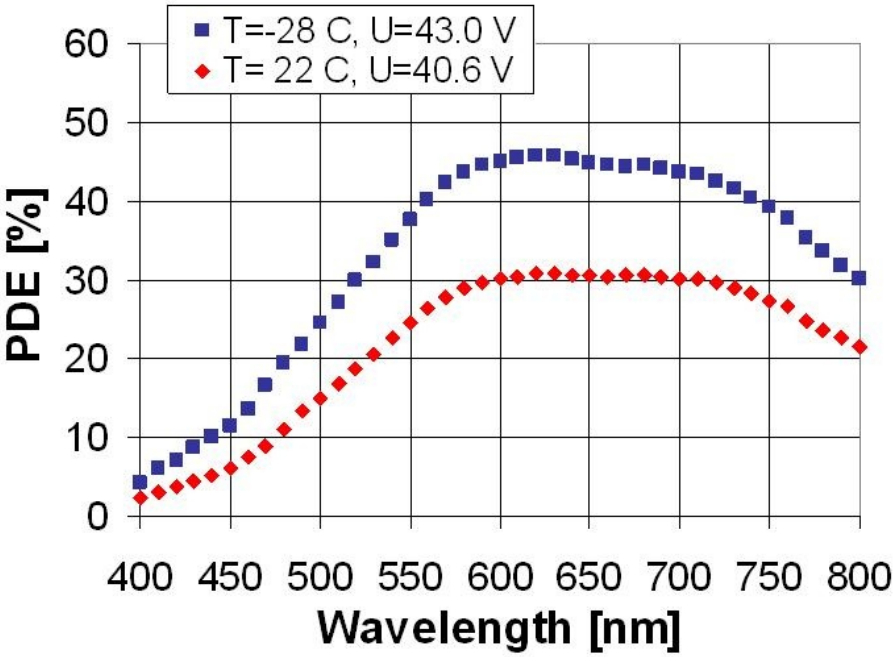

Fig. 8. Photon detection efficiency (PDE) of the 1-mm SiPM [19].

3.4 Custom Power Supply Measurements

We made a series of measurements using the custom high voltage supply developed for use with CMS HCAL PMTs. This power supply had a high voltage ripple of 100 mV. Although not designed to operate at low voltage, this power supply allowed a useful comparison to be made with the better regulated Keithley supply. The data collected with the custom power supply did not use the 10 pf blocking capacitors (see Fig. 4).

Figure 9 shows a scope trace of the signal voltage *vs.* time at 5 mv and 10 ns per division with a 2.5 GHz sampling rate.

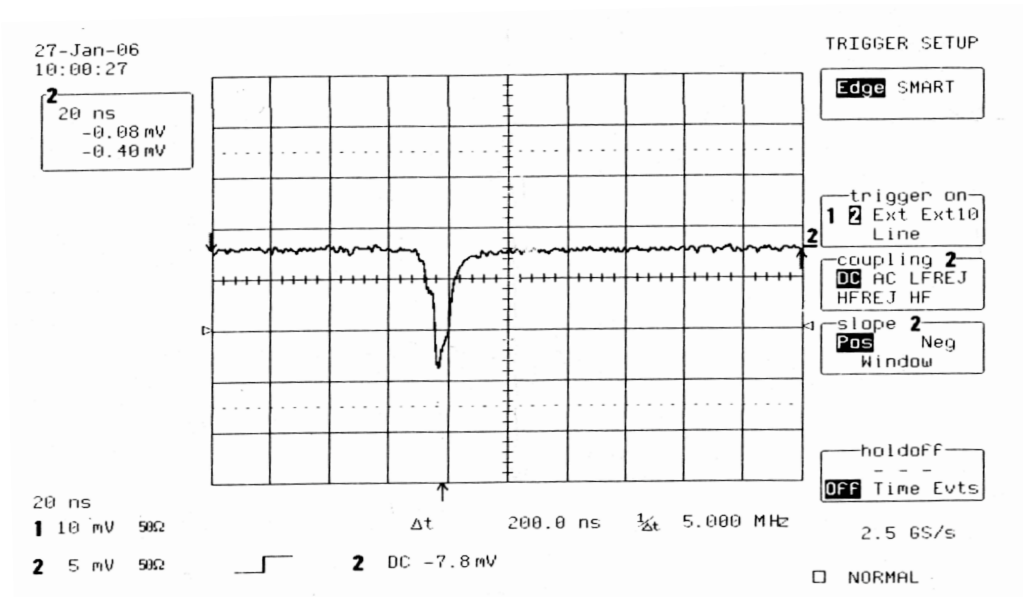

Fig. 9. Signal voltage *vs.* time from the 1-mm^2 SiPM observed with a Lecroy 9361 digital oscilloscope, at 5 mv and 20 ns per division with a 2.5 GHz sampling rate.

Figure 10 shows the charge collected in two consectutive 25-ns QIE time samples using the custom supply for the bias voltage. The bias voltage was $V_\mathrm{b} = 39.6$ V and the current was $I_\mathrm{b} = 1.0$ μA. The effect of the voltage stability (100 mV *vs.* 150 μV) is evident when comparing the separation of the single PE peaks in Figs. 7b) and 10. The QE is higher in Figs. 7 due to the higher voltage ($V_\mathrm{b} = 41.8$ V), but the mean number of PE is similar for the two plots due the attenuation from the 10 pF blocking capacitors.

Figure 11 shows the measured charge distribution with the relative intensity of LED light ouput approximately tripled. The average number of PE has increased from approximately 2 (Fig. 10) to 6. In Figure 11a), where two consecutive 25-ns QIE time samples are summed, the effect of QIE nonlinear quantization is dramatic. Due to the nonlinear scale, there are certain charge combinations in the addition of two time samples that are suppressed. This

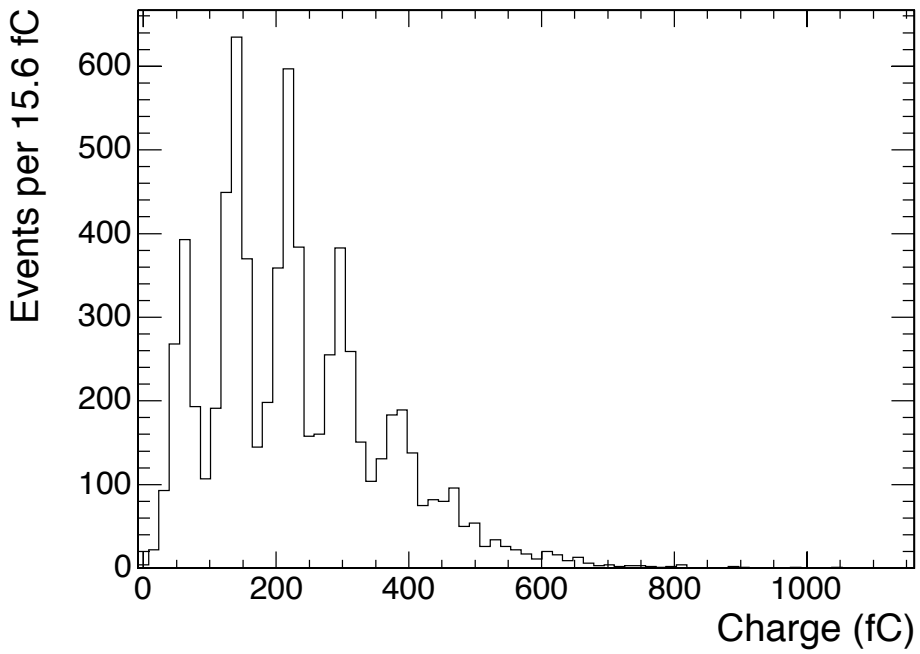

Fig. 10. Charged collected in 2 25-ns QIE time samples with an LED delivering light to the 1-mm^2 SiPM. The bias voltage provided by the custom power supply was $V_\mathrm{b} = 39.6$ V and the current was $I_\mathrm{b} = 1.0$ μA. No blocking capacitors were used.

occurs, for example, when one of the time samples has a large signal so that the bin size is comparable to the width of the PE peak (see Table 2). By summing four consecutive 25-ns time samples as shown in Fig. 11b), the effect of the QIE quantization is averaged out for lower values of total charge.

a)

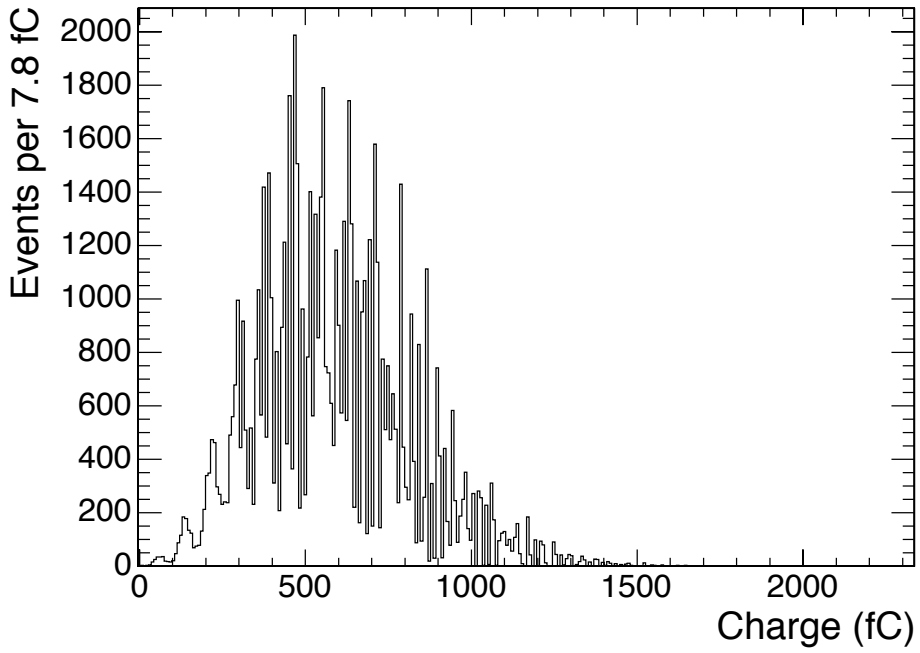

b)

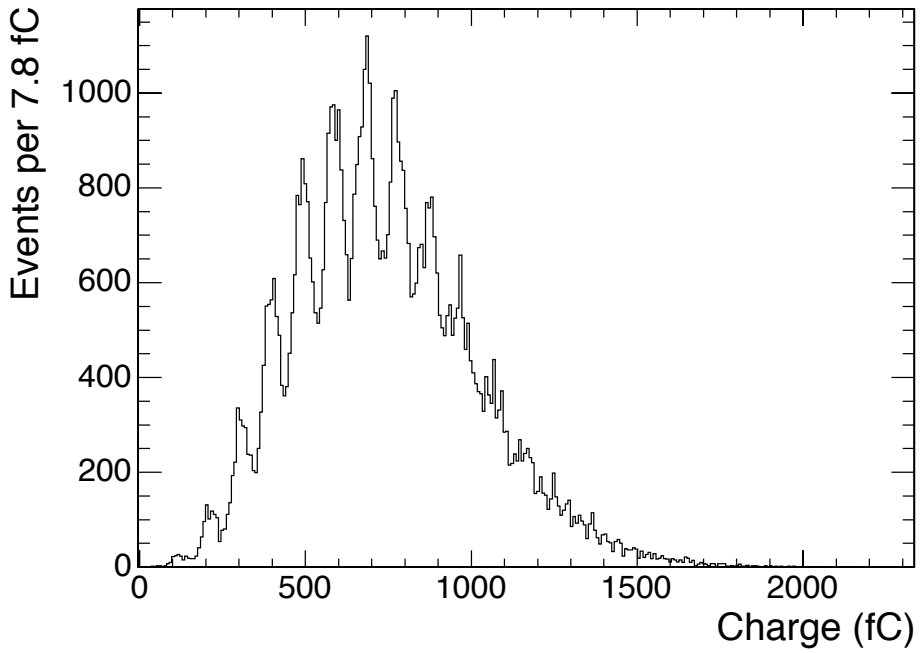

Fig. 11. Charge distributions from the 1-mm^2 SiPM produced with a larger LED pulse relative to Fig. 10. The SiPM bias voltage was $V_{\rm b} = 39.6$ V and the current was $I_{\rm b} = 1.0$ μA. a) Two time samples are summed. The quantization of the QIE has a large effect. b) Four time samples are summed so that the effect of the QIE quantization is averaged out.

3.5 Bias Voltage Dependence

We varied the bias voltage as a means to investigate the signal to noise in the 1-mm SiPM. These data were taken with the custom supply. Figure 12 shows the noise distributions, summed over two consecutive 25-ns QIE time samples, at four different values of bias voltage and resulting current: a) $V_\mathrm{b} = 37.6$ V and $I_\mathrm{b} < 0.25\mu$A b) $V_\mathrm{b} = 38.6$ V and $I_\mathrm{b} = 0.25\mu$A, c) $V_\mathrm{b} = 39.6$ V and $I_\mathrm{b} = 1\mu$A, d) $V_\mathrm{b} = 40.6$ V, $I_\mathrm{b} = 1.75\mu$A. With increasing bias voltage, the pedestal width and dark noise are both observed to significantly increase. The pedestal widths are 10.9 ± 0.3 fC at $V_\mathrm{b} = 37.6$ V, 12.2 ± 0.3 fC at $V_\mathrm{b} = 38.6$ V, 15.5 ± 0.4 fC at $V_\mathrm{b} = 39.6$ V, and 21.5 ± 0.4 fC at $V_\mathrm{b} = 40.6$ V.

Figure 13 shows the charge distribution summed over two consecutive QIE samples for the same four bias voltages: a) $V_\mathrm{b} = 37.6$ V, b) $V_\mathrm{b} = 38.6$ V, c) $V_\mathrm{b} = 39.6$ V, and d) $V_\mathrm{b} = 40.6$ V. One sees the expected effect that the single PE separation increases with bias voltage as does the quantum efficiency. At sufficiently high bias voltage, however, the signal to noise and the dark count will degrade even though the quantum efficiency continues to rise.

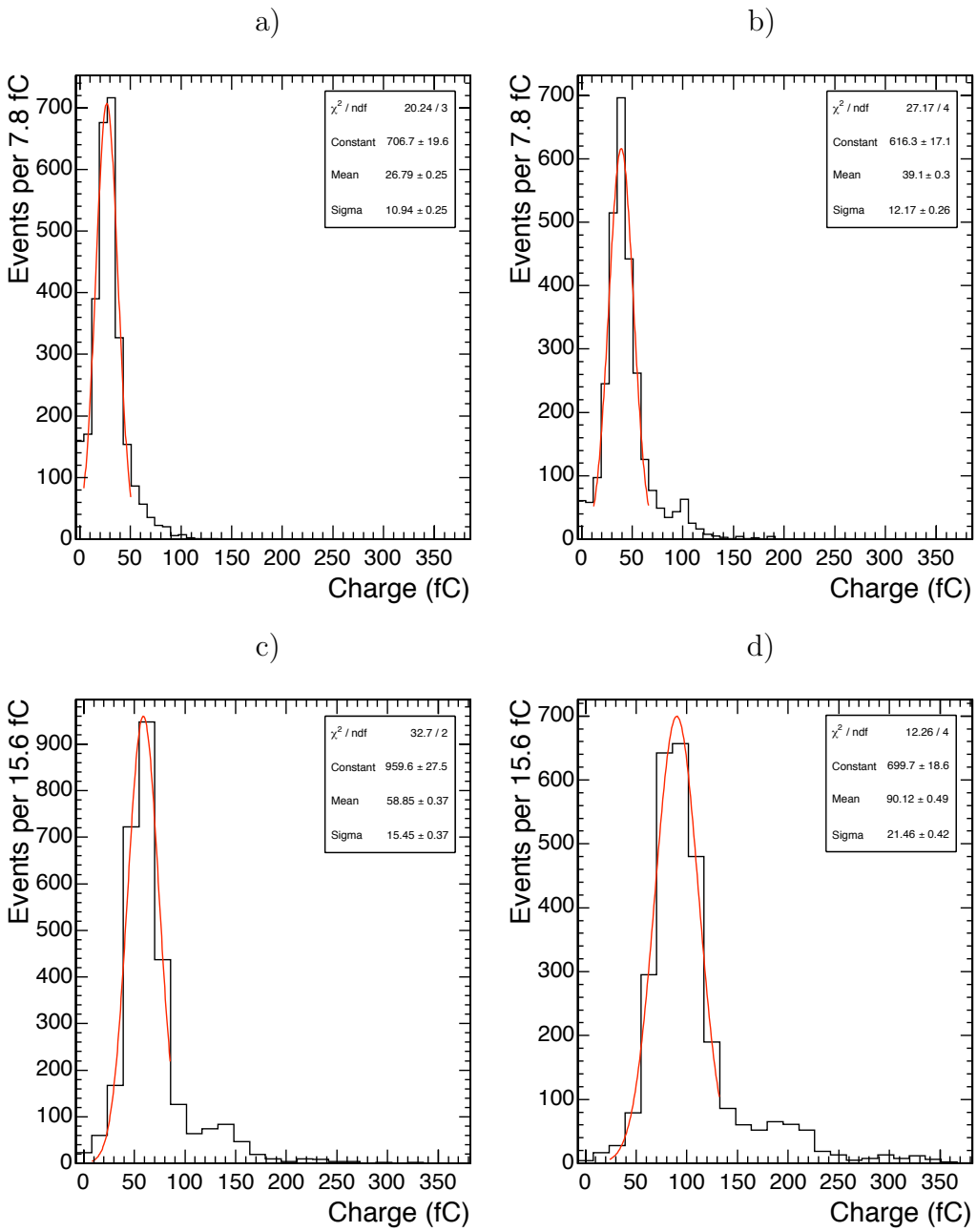

Fig. 12. Dependence of pedestal charge distributions on bias voltage: a) $V_{\mathrm{b}} = 37.6$ V and $I_{\mathrm{b}} < 0.25\mu$A b) $V_{\mathrm{b}} = 38.6$ V and $I_{\mathrm{b}} = 0.25\mu$A, c) $V_{\mathrm{b}} = 39.6$ V and $I_{\mathrm{b}} = 1\mu$A, d) $V_{\mathrm{b}} = 40.6$ V, $I_{\mathrm{b}} = 1.75\mu$A.

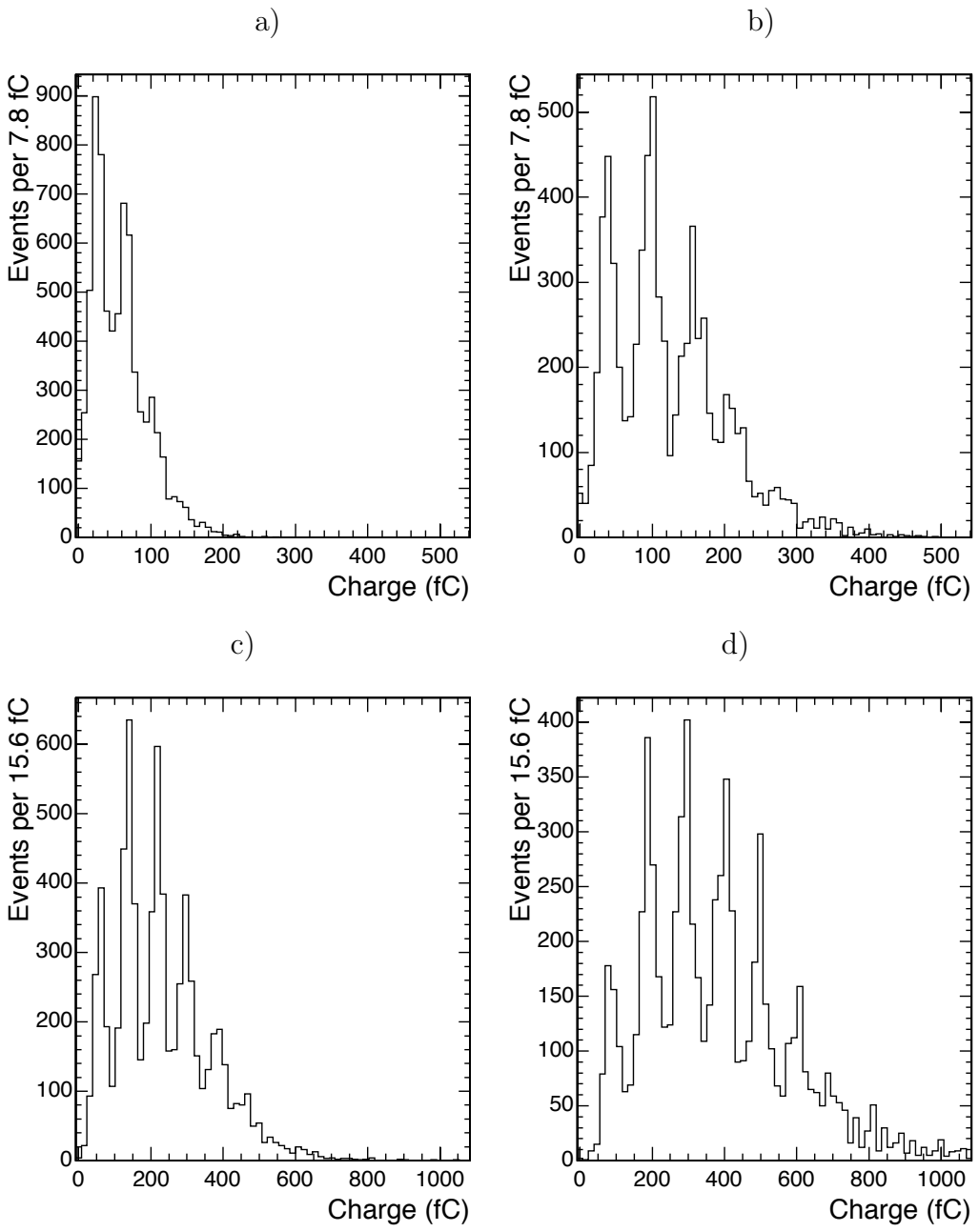

Fig. 13. Charge distribution in two consecutive QIE time samples for different bias voltages a) $V_{\mathrm{b}} = 37.6$ V, b) $V_{\mathrm{b}} = 38.6$ V, c) $V_{\mathrm{b}} = 39.6$ V, and d) $V_{\mathrm{b}} = 40.6$ V.

4 4 × 1-mm^2 SiPM

For many applications it may be desirable to increase the photosensitive area of the SiPM. For example, the CMS HCAL outer calorimeter scintillators have light collected in four 1-mm diameter optical fibers. We have investigated a larger device (4 × 1-mm^2 SiPM) which is a 2×2 mosaic of the 1-mm SiPM in a single unit as shown in Fig. 14. Figure 15 shows a a scope trace of the signal voltage *vs.* time at 5 mv and 20 ns per division with a 2.5 GHz sampling rate. Compared to the 1-mm SiPM (Fig. 9) , the 4 × 1-mm^2 SiPM is significantly slower due to its increased capacitance.

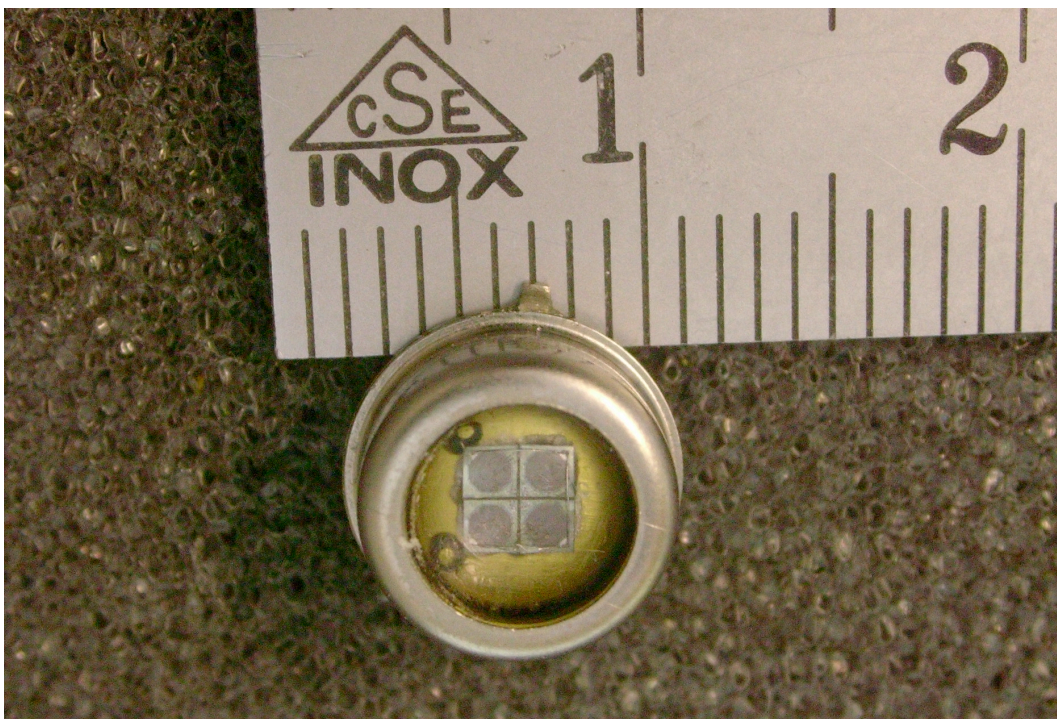

Fig. 14. The 4 × 1-mm^2 SiPM.

Figure 16 shows the noise distribution from the 4 × 1-mm^2 SiPM. The bias voltage (using the custom power supply and no blocking capacitors) and current were $V_\mathrm{b} = 40.1$ V and $I_\mathrm{b} = 3.25$ μA. A Gaussian fit to the zero-PE peak gives a mean of 150 fC and an rms width of 20.3 ± 0.3 fC.

Figure 17 shows the signal from the 4 × 1-mm^2 SiPM when pulsed with the LED and read out with the QIE electronics. The bias voltage and current (using the custom power supply and no blocking capacitors) were $V_\mathrm{b} = 40.1$ V and $I_\mathrm{b} = 3.25$ μA. Figure 17a) shows the QIE time distribution and Fig. 17b) shows the charge distribution collected in two consecutive time samples (10 and 11). The single-PE peak has a width of 26.5 ± 1.2 fC.

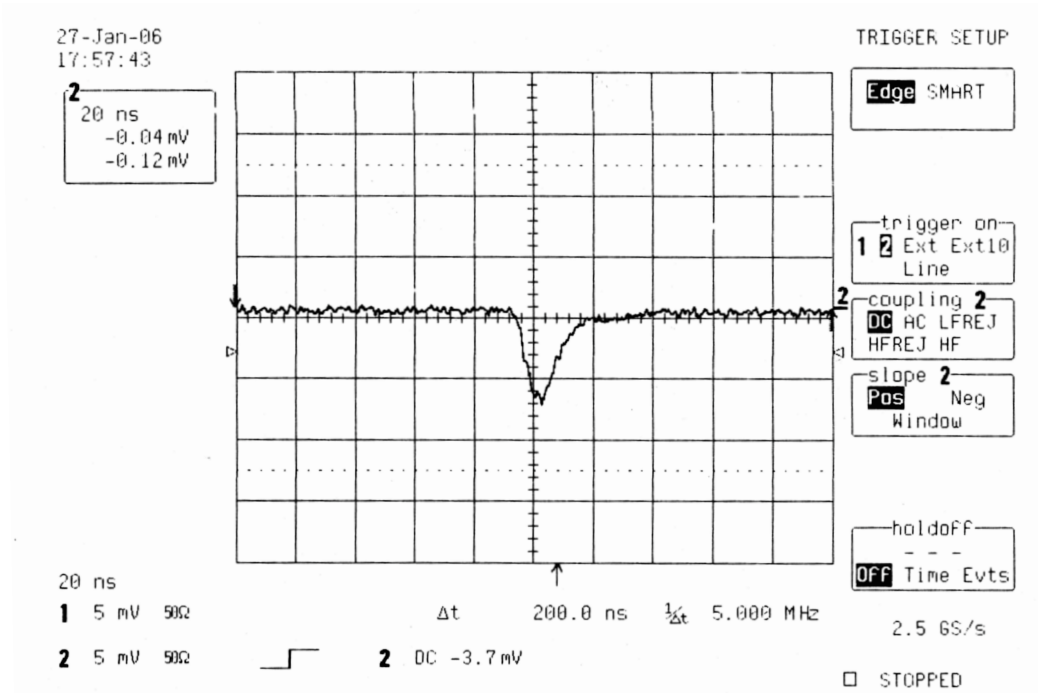

Fig. 15. Signal voltage *vs.* time from the 4×1-mm^2 SiPM observed with a Lecroy 9361 digital oscilloscope, at 5 mv and 20 ns per division with a 2.5 GHz sampling rate.

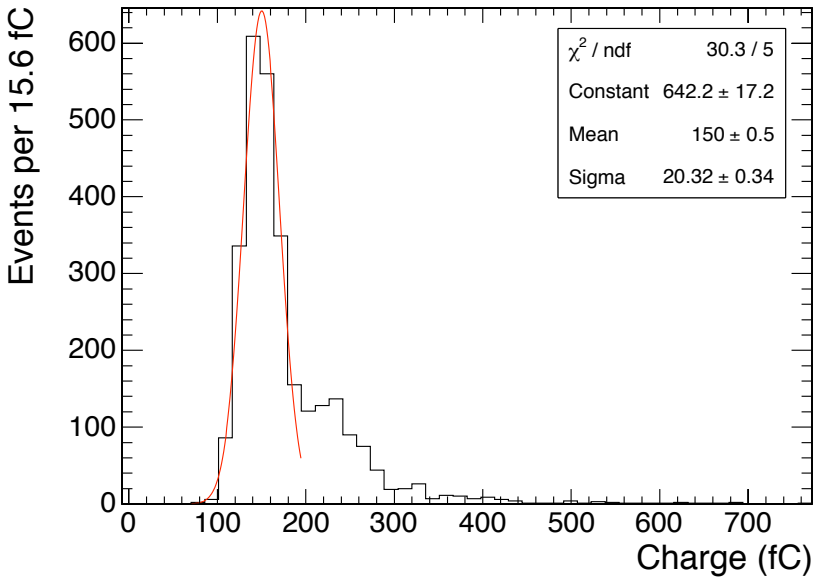

Fig. 16. Pedestal charge (Q) distribution from the 4×1-mm^2 SiPM measured with the QIE. The bias voltage and current were $V_\mathrm{b} = 40.1$ V and $I_\mathrm{b} = 3.25$ μA. A Gaussian fit (curve) to the zero-PE peak gives a mean of 150 fC and an rms width of 20.3 ± 0.3 fC.

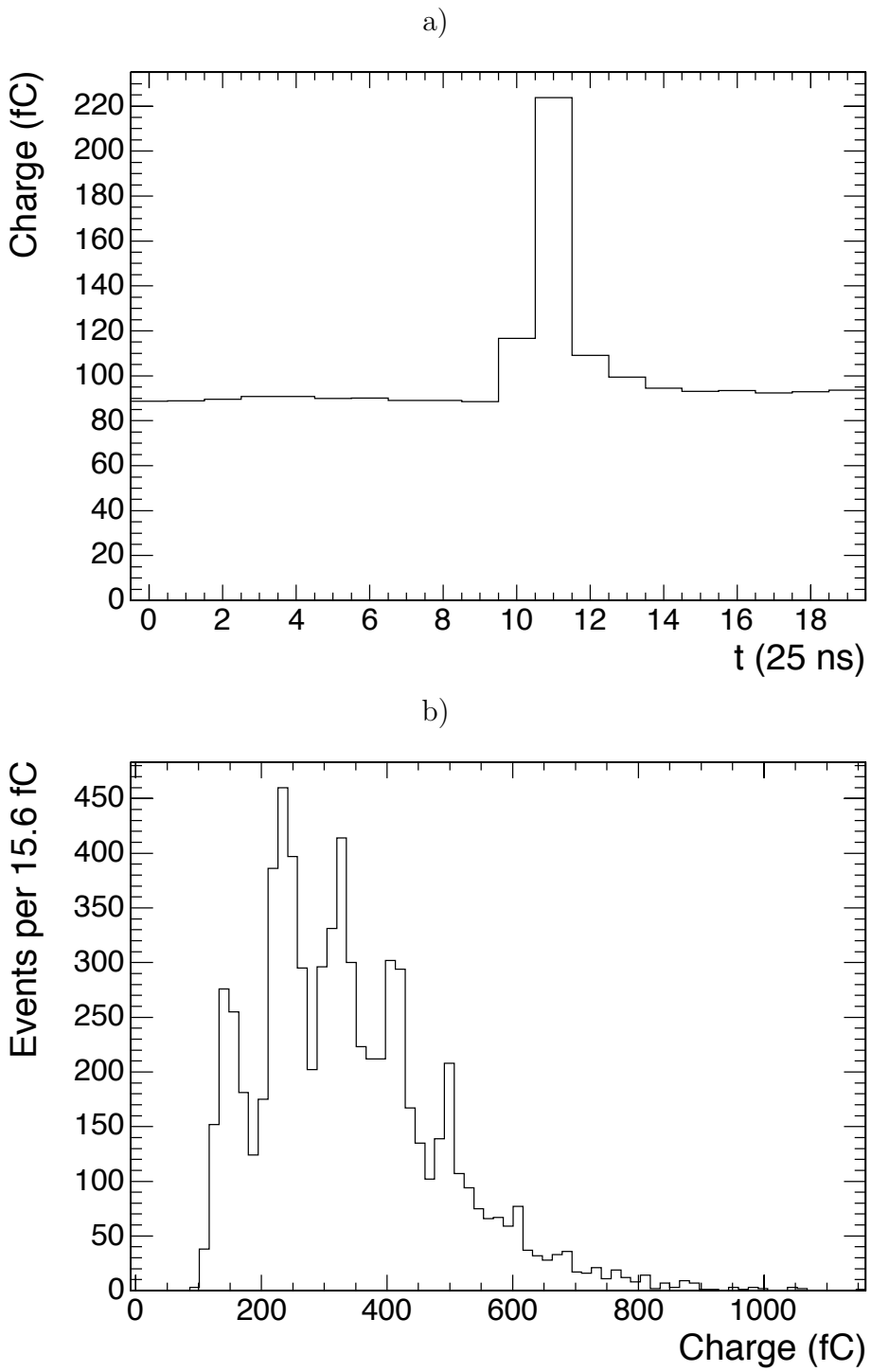

Fig. 17. Average pulse shape, charge (Q) *vs.* time (t), from the 4×1-mm^2 SiPM read through the QIE electronics. The digitization is at 40 MHz and 20 25-ns time samples are recorded. The bias voltage and current were $V_\mathrm{b} = 40.1$ V and $I_\mathrm{b} = 3.25$ μA. a) Charge *vs.* time collected in 25-ns time samples. b) Charge distribution collected in time samples 10 and 11, showing clear peaks for 0, 1, 2, 3, and 4 photoelectrons.

5 Summary

The data collected here are summarized in Table 3. The rms noise is defined as the width of the pedestal distribution summed over two consecutive QIE time slices. The gain is calculated as the location of the single PE peak above the pedestal zero-PE peak. The single-PE signal-to-noise (1 PE / noise) is calculated as the gain divided by the rms noise. The data show that a signal to noise in excess of 8 may be achieved with the SiPM. For use in reading out the CMS HCAL outer scintillators, this would correspond in improvement in signal-to-noise by about a factor of 4 and greatly enhance their usefulness as part of the muon RPC trigger.

Table 3
Measured device characteristics. The data taken with the custom supply did not use blocking capacitors while the data with the Keithley supply used 10 pF blocking capacitors (Fig. 4) resulting in an attenuation of a factor of 5.

Device	V_b (V)	I_d (μA)	rms noise (fC)	gain (fC/PE)	1 PE / noise
1-mm^2 SiPM	37.6	< 0.25	10.9	38	3.5
(Custom supply)	38.6	0.25	12.2	58	4.8
	39.6	1.0	15.5	80	5.2
	40.6	1.75	21.5	100	4.7
1-mm^2 SiPM	40.8	1.25	2.4	21	8.7
(Keithley supply)	41.8	2.2	3.6	27	7.5
$4 \times$ 1-mm^2 SiPM	40.1	3.25	20.3	88	4.3
(Custom supply)					

6 Ackowlegement

We thank John Elias for many useful comments.

References

[1] For example, in the Compact Muon Solenoid experiment for the CERN Large Hadron Collider, the electromagnetic crystal calorimeter is read out with APDs, J. Grahl *et al.*, "Radiation hard avalanche photodiodes for CMS ECAL," Nucl. Instrum. Meth. A504 (2003) 44 and the scintillator tile hadron calorimeter is read out with HPDs, P. B. Cushman and A. H. Heering, "Problems and solutions in high-rate multichannel hybrid photodiode design: The CMS experience", IEEE Trans. Nucl. Sci. 49 (2002) 963.

[2] P. Buzhan *et al.*, "Silicon photomultiplier and its possible applications," Nucl. Instr. and Meth. A504 (2003) 48.

[3] A. Akindinov *et. al*, "Prototype of a cosmic muon detection system based on scintillation counters with MRS APD light readout," Nucl. Instr. Meth. A555 (2005) 65.

[4] A. Akindinov *et al.*, "Scintillation counter with MRS APD light readout," Nucl. Instr. and Meth. A539 (2005) 172.

[5] A. Akindinov *et al.*, "Detection of Light Pulses Using an Avalanche-Photodiode Array with a MetalResistorSemiconductor Structure," Instrum. Exp. Tech 48 (2005) 355.

[6] P. Buzhan *et al.*, "The Advanced Study of Silicon Photomultiplier," ICFA Instumentation Bulletin, Fall 2001, http://www.slac.stanford.edu/pubs/icfa/fall01.html.

[7] E. Aprile, P. Cushman, K. Ni, and P. Shagin, "Detection of liquid xenon scintillation light with a silicon photomultiplier," Nucl. Instrum. Meth. A556 (2006) 215.

[8] N. Otte *et al.*, "The Potential of SiPM as Photon Detector in Astroparticle Physics Experiments like MAGIC and EUSO," Nucl. Phys. Proc. Suppl. 150 (2006) 144.

[9] "CMS, The Hadron Calorimeter Technical Design Report," CERN/LHCC 97-31 CMS TDR 2 (June 1997).

[10] "CMS Technical Proposal," CERN/LHCC 94-38, LHCC/P1 (December 1994).

[11] "The Large Hadron Collider: Conceptual Design," CERN/AC/95-05 (LHC) (Oct. 1995), http://doc.cern.ch/archive/electronic/other/preprints//CM-P/cm-p00047618.pdf.

[12] C. Albajar *et al.*, "Conceptual Design of an Improved CMS RPC Muon Trigger Using the Hadron Outer Scintillators," Nucl. Inst. Meth. A545, 97 (2005).

[13] J. Rohlf, "Super-LHC: The Experimental Program," talk given at the International Workshop on Future Hadron Colliders (2003) http://conferences.fnal.gov/hadroncollider/talks/rohlf.pdf

[14] J. Freeman, "Calorimeters for the SLHC and VLHC," talk given at the International Workshop on Future Hadron Colliders (2003) http://conferences.fnal.gov/hadroncollider/talks/freeman.pdf

[15] Center of Perspective Technologies and Apparatus (CPTA). Preobrazhenskaya pl. 6/8, Moscow, 107076 RUSSIA http://www.slac.stanford.edu/spires/find/institutions/www?icncp=CPTA,+Moscow

[16] T. Zimmerman and M. Sarraj, "A Second Generation Charge Integrator and Encoder ASIC," IEEE NS V433 (June 1996).

[17] T. Zimmerman and J. R. Hoff, "The Design of a charge integrating, modified floating point ADC chip," IEEE J. Solid State Circuits, 39 (2004) 895.

[18] T. Zimmerman, A. Baumbaugh, J. Hoff, S. Los, and T. Shaw, "Specification for Production CMS QIE ASIC (QIE8)," Fermilab Particle Physics/Electrical Engineering Department (2002), http://www.uscms.org/scpac/Detector/HCAL/calib/data/qie/020903-scale/qie_spec.pdf

[19] E. Guschin *et al.*, "Multi-pixel Geiger-mode avalanche photodiodes with high quantum efficiency and low excess noise factor," poster presented at the 3rd International Conference on New Developments in Photodetection, Beaune, France (June 17-21, 2002), Nucl. Inst. Meth. in press.